nature energy

ARTICLES

https://doi.org/10.1038/s41560-020-00680-x

Ambient-pressure and low-temperature upgrading of lignin bio-oil to hydrocarbons using a hydrogen buffer catalytic system

Wei Liu, Wenqin You, Wei Sun, Weisheng Yang, Akshay Korde, Yutao Gong and Yulin Deng ✉

Catalytic hydrodeoxygenation is an essential step for bio-oil upgrading. However, hydrodeoxygenation usually requires a high hydrogen pressure and high temperature due to the good stability of the C–O bonds. Here we report an effective multiphase hydrodeoxygenation of lignin-based bio-oil at temperatures <100 °C and hydrogen pressures <1 atm using a synergetic catalyst system that consists of a low redox potential $H_4SiW_{12}O_{40}$ (SiW_{12}) and suspended Pt-on-carbon (Pt/C) particles. We propose that SiW_{12} plays three critical roles in bio-oil hydrodeoxygenation. First, it quickly oxidizes the H_2 gas to form reduced SiW_{12} in the presence of Pt/C. Second, it transfers both electrons and H^+ ions to the bulk phase to form active H* or H_2 on the Pt/C surface. Third, the formation of the oxonium ion in a SiW_{12} superacid solution reduces the deoxygenation energy. The SiW_{12}-enhanced proton-transfer hydrodeoxygenation mechanism is supported by density functional theory computations. As a result of the hydrogen buffer and acidic effect, up to a 90% yield of hydrocarbons (cyclohexane, benzene and their derivatives) was achieved from the hydrodeoxygenation of phenol and its derivatives.

Lignocellulosic biomass-derived bio-oil is a potential next-generation fuel that can be extracted from renewable and sustainable resources and has an energy density higher than that of biomass itself[1–3]. The bio-oil is produced by the decomposition of polymeric biomass into small molecular oxygenates, such as aldehydes, ketones, carboxylic acids and phenols, using pyrolysis or liquefication methods under a high temperature[4,5]. To obtain stable bio-oils that work in the desired temperature range with a reasonably high heat value, oxygen atoms in the bio-fuel molecules must be removed, commonly through catalytic hydrodeoxygenation (HDO)[6–8]. However, conventional catalytic HDO is conducted under high reaction temperatures (~200–500 °C) and high hydrogen pressures (~2–200 bar) (refs. [8–10]), which is an energy-intensive process. A recent review of the catalytic conversion of lignin-derived monomers that involve hydrogen on different HDO sites (such as Ru, Pt, Pd, Rh, Nb and Mo) showed that all the reactions were performed under high temperatures and high hydrogen pressures[11].

Upgrading raw bio-oil to hydrocarbon fuels under mild conditions (low temperature and low hydrogen pressure) is a difficult challenge because of the high dissociation energy required to break the aromatic C–O bonds (~468 kJ mol^{-1}) (refs. [12,13]). A high temperature is generally needed to cleave the C–O bond, but it causes char or tar formation and catalyst deactivation, which seriously restrict the reactions. A high H_2 pressure is commonly required in a traditional hydrogenation process. Hydrogen plays important roles in the HDO, which include hydrogenation of unsaturated bonds, deoxygenation of C–O bonds to yield C–H bonds and hydrocracking of C–C bonds to produce low-molecular-weight compounds. It can also adjust the active site of the catalyst by reducing the active metal and producing active oxygen vacancies on the metal oxide[11,14]. As H_2 solubility in the aqueous phase is extremely low, increasing the concentration of hydrogen is critically important to improve the HDO efficiency in the liquid-phase reaction. Therefore, it is expected that if an effective hydrogen carrier that can transfer H_2 from the gas phase to a liquid one is used, the HDO reaction in the liquid phase could be much improved.

Here we present a synergetic bifunctional triphase hydrogen-transfer catalytic system to drive HDO in water under mild conditions. In our bifunctional catalytic system, we used a low redox potential polyoxometallate acid, $H_4SiW_{12}O_{40}$ (SiW_{12}), as the hydrogen buffer and carrier, and we suggest this SiW_{12} can quickly transfer hydrogen gas from the gas–liquid interphase into the bulk solution via a reversible hydrogen extraction, and then release hydrogen as an active species H* on the Pt/C surface. Our calculations indicate that the super acidity of polyoxometallate greatly decreases the activation energy for the deoxygenation through a proton-associated dehydration reaction. Therefore, even under an extremely low hydrogen pressure (<1 atm) and simultaneous low reaction temperature (<100 °C), efficient HDO successfully occurs and high yields of hydrocarbons are achieved.

The hydrogen buffer effect

It is a great challenge to remove the oxygen atoms from lignin-derived oil compounds to produce hydrocarbon products under low temperature and hydrogen pressure (Fig. 1a). To increase the H_2 gas transfer to the liquid solution under ambient pressure, a low redox potential polyoxometallate acid, SiW_{12}, was dissolved in water, and the required Pt/C catalyst particles were added. SiW_{12} is composed of the Keggin-structured $[SiW_{12}]^{4-}$ anions and four protons that can be completely dissociated in aqueous solution. Without Pt/C, no obvious reaction between the $[SiW_{12}]^{4-}$ anions and H_2 occurred at the gas–liquid interface. However, by adding a small amount of Pt/C particles into the water phase, a quick colour change of the solution from colourless $[SiW_{12}]^{4-}$ to deep blue $[SiW_{12}]^{5-}$ was observed when H_2 gas was bubbled into the solution, which indicates a quick reaction between SiW_{12} and H_2 in the presence of Pt/C (Supplementary Fig. 1). Owing to the low standard redox potential of $[SiW_{12}]^{4-}$/$[SiW_{12}]^{5-}$, $E°=-0.05$ V versus the normal hydrogen electrode (NHE))[15], which is close to that of H^+/H_2, a reversible reduction of

School of Chemical & Biomolecular Engineering and RBI, Georgia Institute of Technology, Atlanta, GA, USA. ✉e-mail: yulin.deng@rbi.gatech.edu

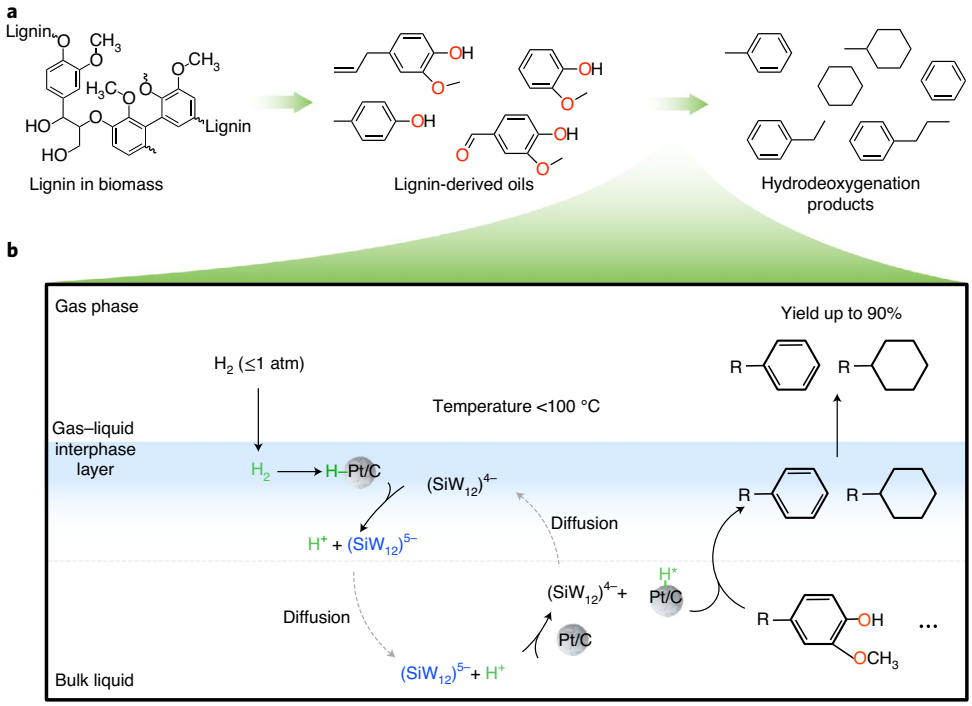

Fig. 1 | Illustration of hydrogen-buffer-improved bio-oil upgrading. a, The common structures of lignin, lignin-derived bio-oil and hydrocarbon products after upgrading. **b**, Illustration of the proposed reaction of SiW_{12} hydrogen buffer, which transfers hydrogen gas into the solution over a Pt/C catalyst for HDO.

$[SiW_{12}]^{4-}$ by H_2 occurred at the Pt/C surface, as shown in Fig. 1b and equation (1):

$$1/2H_2 + [SiW_{12}]^{4-} \overset{Pt}{\rightleftharpoons} H^* + [SiW_{12}]^{4-} \overset{Pt}{\rightleftharpoons} H^+ + [SiW_{12}]^{5-} \quad (1)$$

As a result, equilibriums between $[SiW_{12}]^{4-}$, $[SiW_{12}]^{5-}$, H^+, H^* and H_2 were reached. Also, note that $[SiW_{12}]^{5-}$ is very stable under an inert-gas environment in water unless it and H^+ are simultaneously absorbed on the Pt surface. Therefore, SiW_{12} is a good H_2 carrier or buffer, which quickly reacts with hydrogen at the gas–liquid interphase and transfers it into the bulk solution to generate H^* over the Pt/C surface (the reverse reaction). This process is equivalent to an increase in the solubility of hydrogen gas in water.

To investigate the redox potential changes of the SiW_{12} solution during the reactions described above, hydrogen electrode potential measurements were conducted. We employed a Pt black electrode coupled with a reference electrode to monitor the potential in the reaction of SiW_{12} and H_2 over a Pt/C catalyst (the experimental set-up is shown in Supplementary Fig. 1). To make a comparison, SiW_{12} was first replaced by a H_3PO_4 solution. As shown in Fig. 2a (blue curve), the electrode potential dramatically dropped when H_2 gas was purged into the open reactor chamber. This is because of the hydrogen adsorption and discharging on the Pt black electrode in H_3PO_4 solution. By switching to N_2 purging, the electrode potential gradually increased to the initial state because of the desorption of H_2.

Unlike the H_3PO_4 solution, SiW_{12} reacts with hydrogen to yield a reduced form with a Pt/C catalyst. At the beginning of H_2 purging, the reaction moves towards the right side of equation (1) to form $[SiW_{12}]^{5-}$. The reduction of the $[SiW_{12}]^{4-}$ ion by H_2 was verified by the colour change of the solution from colourless to dark blue and the simultaneous sluggish drop of the electrode potential change in the first four minutes (red curve in Fig. 2a). The formed moles of $[SiW_{12}]^{5-}$ ions can be calculated by spectrophotometric analysis of the solution absorbance at 700 nm based on its linear relationship with the concentration of reduced ions $[SiW_{12}]^{5-}$ (Supplementary Fig. 2). As the H_2 gas was purged into the SiW_{12} solution, the pH value of the solution gradually decreased because the hydrogen dissociated in the solution and then was oxidized to give protons (equation (1) and Supplementary Fig. 3). As 1 mol of SiW_{12} transfers 0.5 mol of H_2 to the solution, the amount of H_2 that is transferred from the gas phase to the solution phase can be calculated. Note that this absorbed hydrogen gas can be released as active H^* or H_2 inside the bulk solution on the Pt/C surface, which is equivalent to increasing the solubility of H_2 in the liquid phase. The analysis of the $[SiW_{12}]^{5-}$ concentration in the solution indicates that the hydrogen gas transfer rate could reach up to 40 N cm^3 min^{-1} (N, normal) with a SiW_{12} concentration of 0.05 mol l^{-1} at 20 °C.

With continuous H_2 purging, the reduction reached equilibrium after about three minutes, as shown in Fig. 2a. At equilibrium, we measured that 91% of the $[SiW_{12}]^{4-}$ ions had reduced to $[SiW_{12}]^{5-}$ under these experimental conditions. As a result, the $[SiW_{12}]^{5-}$ concentration and measured electrode potential remained stable in the equilibrium, due to the reversibility of the reaction.

After the H_2 gas was replaced by purging of N_2, the SiW_{12} catalytic system was maintained at the low electrode potential for a long time (red curve in Fig. 2a). However, the reverse reaction of the SiW_{12} reduction, that is, hydrogen gas release from $[SiW_{12}]^{5-}$ ions, gradually occurs. The redox reversibility of SiW_{12}, as shown in equation (1), was verified by cyclic voltammetry, which showed a reversible one-electron redox peak centred at +0.01 V versus NHE (Supplementary Fig. 4). Hydrogen evolution from reduced $[SiW_{12}]^{5-}$ ions has previously been verified by electrolysis[16]. Our experiments measured that 1.9 ml of H_2 was released in 40 minutes from 10 ml of 0.05 mol $^{l-1}$ prereduced SiW_{12} solution at 20 °C (Supplementary Fig. 5). The evolved hydrogen volume is ten times higher than the hydrogen solubility in water at 1 atm and 20 °C (0.18 ml of H_2 in

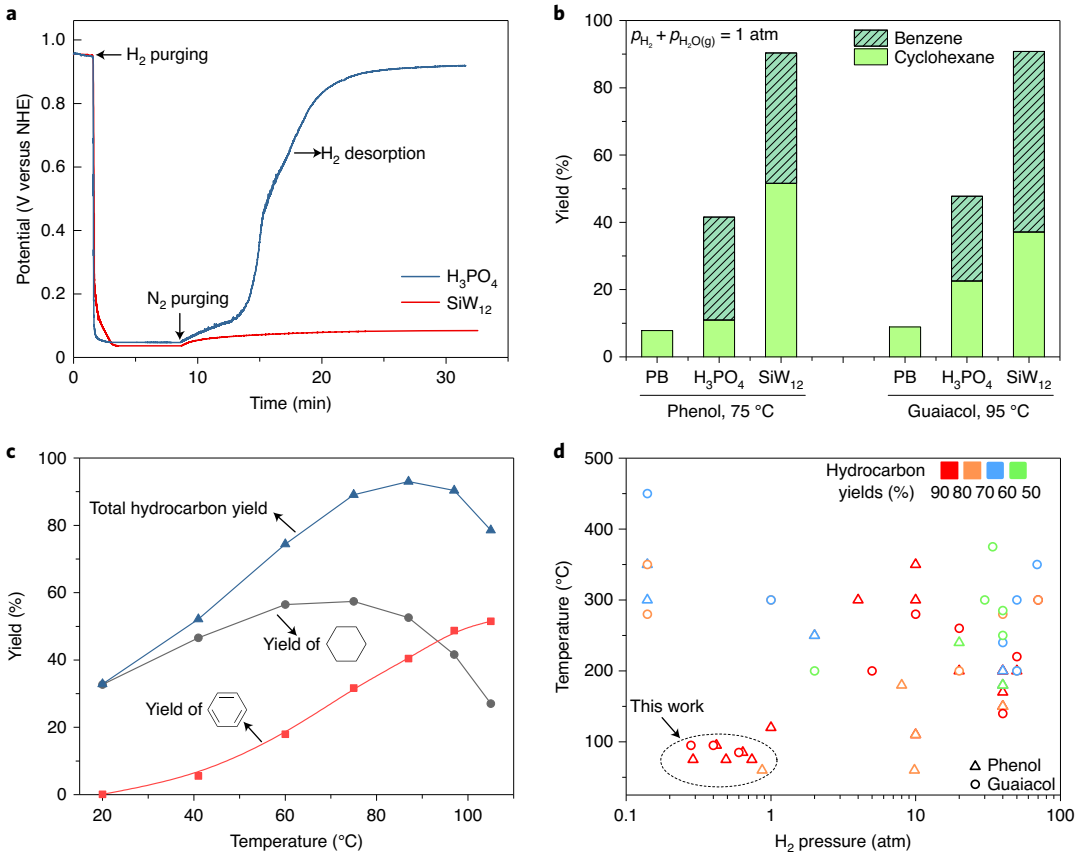

Fig. 2 | The hydrogen buffer effect and HDO performance of the SiW_{12} and Pt/C catalyst system. a, Electrode potential changes during the H_2 purging in the SiW_{12} and H_3PO_4 catalytic system. **b**, In Fig. 2b, comparison of hydrocarbon yields in the PB (pH = 7), H_3PO_4 and SiW_{12} catalytic systems for phenol (at 75 °C for 30 min) and guaiacol (at 95 °C for 35 min) HDO (initial organic substrate concentration, 0.02 mol l^{-1}; Pt to substrate, 5 mol%; details in Supplementary Tables 1 and 2). Yields of CH_4 were less than 1%, and are neglected here. The total pressure ($p_{H_2} + p_{H_2O(g)}$ in the reaction container) was maintained at 1 atm. **c**, HDO of phenol under different temperatures. The H_2 partial pressure was measured at ambient temperature. **d**, Comparison of HDO conditions in this study and with reports in the literature (Supplementary Tables 4 and 5)[8,11,12,14,21,25–28,37].

10 ml of water), which is the equivalent of increasing the hydrogen pressure to 10 atm by using a 0.05 mol l^{-1} SiW_{12} reaction solution.

HDO performance under mild conditions

HDO reactions were performed using phenol and guaiacol as model lignin bio-oil compounds in the presence of SiW_{12} and Pt/C catalysts. The experimental set-up is shown in Supplementary Fig. 6. Besides the SiW_{12} catalytic system, phosphate buffer (PB, pH = 7) and H_3PO_4 were used to replace SiW_{12} in the control experiments. As shown in Fig. 2b, the HDO of phenol with a Pt/C catalyst in PB solution yielded only 7.9% cyclohexane. H_3PO_4 can slightly increase the hydrocarbon yield (results are shown in Supplementary Fig. 7) because the hydronium ion in solution can reduce the hydrogen binding energy on the Pt catalyst and thus improve the HDO reaction[17,18]. By simply increasing the hydrogen pressure to 10 atm, the H_3PO_4-catalysed phenol hydrogenation obtained an improved performance (Supplementary Fig. 7), and the H_3PO_4–Pt/C catalytic system has also been reported as an effective HDO system at 200 °C and 20–50 atm H_2 pressure[19,20]. Figure 2b indicates that the total yield of hydrocarbons, which includes cyclohexane and benzene, is about 40% at ambient hydrogen pressure and a temperature of around 75 °C for phenol. Compared with the reported results performed under similar hydrogen pressure and temperature, our H_3PO_4–Pt/C system shows slightly higher hydrocarbon yields[21–24], which is possibly because a higher acidity condition was used in our tests. Previously, it was reported that the activation energy of H_2 gas dissociation into hydrogen atoms in water could be lowered by increasing the acidity of the solution[18]. However, it is difficult to improve the hydrocarbon yield further using a simple H_3PO_4–Pt/C system by increasing the acidity. Instead, hydrogen pressure plays a dominating role in further improving the reaction yield under a low reaction temperature due to the hydrogen-mass-transfer limitation, which was verified by our experiments (Supplementary Fig. 8)

In contrast to the PB and H_3PO_4 solutions, the SiW_{12} and Pt/C catalyst system can quickly incorporate hydrogen gas into the reaction solution via the reversible SiW_{12} reduction under a low hydrogen pressure (as shown in Fig. 1b and equation (1)). As a result, the SiW_{12} and Pt/C catalyst system showed a high yield of 87.7% of the total hydrocarbons during phenol HDO at 75 °C (measured H_2 partial pressure (p_{H_2}) = 0.74 atm), and 83.4% yield during the HDO of guaiacol at 95 °C (measured p_{H_2} = 0.42 atm). Figure 2c shows the hydrocarbon yields of phenol HDO under different temperatures (gas chromatograms of the products are shown in Supplementary Figs. 9–15). Note that the total pressure of water vapour and H_2 in the reactor was controlled at 1 atm. As the water vapour pressure increased when the temperature was elevated, the p_{H_2} in the system decreased if the total pressure was maintained at 1 atm (the p_{H_2} and temperature relationship is shown in Supplementary Fig. 16). The highest total hydrocarbon yield of phenol HDO was 90.8%, which includes 39.3% benzene and 51.5% cyclohexane at a temperature of 85 °C and H_2 partial pressure of 0.64 atm (measured at ambient). The benzene yield increased at elevated temperatures

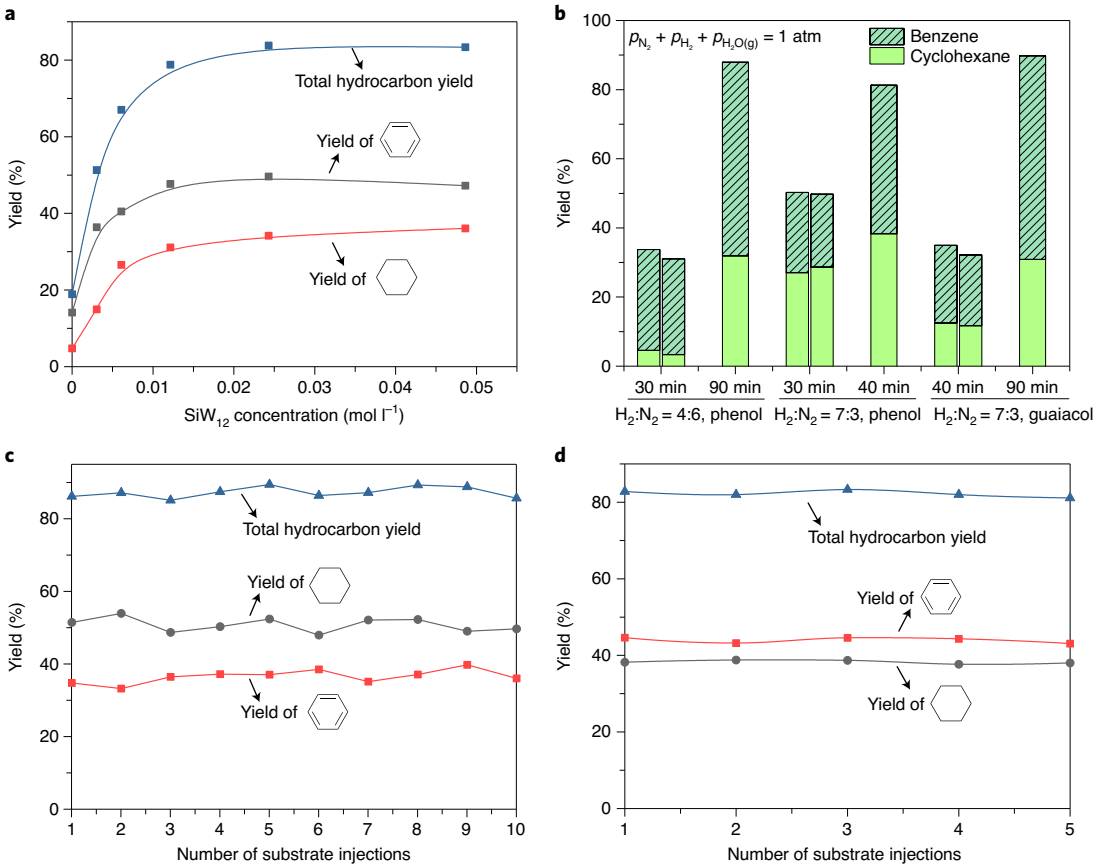

Fig. 3 | HDO of phenol and guaiacol. a, HDO of guaiacol with different SiW_{12} concentrations at 75 °C for 30 min. Curves are fitted by B-splines. **b**, HDOs of phenol (at 75 °C) and guaiacol (at 95 °C) using a N_2 and H_2 mixing gas (total pressure 1 atm). The two bars for the 30 and 40 min tests of phenol and guaiacol, respectively, are test results from two independent experiments. **c**,**d**, The performance of the SiW_{12}–Pt/C catalyst with increased injection numbers of phenol (**c**) and guaiacol (**d**) in the HDOs. The organic substrate was injected into the reaction system at 30 (phenol) or 40 (guaiacol) min intervals in the continuous experiments for the catalyst repetitive performance evaluation (details shown in Methods).

because a high temperature can weaken the aromatic C–O bond. The fully hydrogenated product, cyclohexanol, was produced, but was deoxygenated to give cyclohexane as the reaction progressed (Supplementary Fig. 17). The Pt/C catalyst amount was optimized in the SiW_{12}-mediated phenol and guaiacol reactions to improve the HDO efficiency. The HDO efficiency can be evaluated as the turnover frequency (TOF), which is the rate of phenol conversion or hydrocarbon production in the HDO reactions normalized by the number of surface metal atoms of the Pt/C catalyst (Supplementary Figs. 17 and 18). The TOF value of hydrocarbon production in phenol deoxygenation with the SiW_{12} (0.025 mol l^{-1}) catalytic system achieved 418.2 h^{-1} at a temperature of 75 °C and Pt-to-phenol ratio of 0.25 mol%. The possible competitive adsorption of SiW_{12} and organic substrates on the Pt catalyst surface means that the TOF value is affected by ratios of both Pt to SiW_{12} and Pt to phenol (Supplementary Fig. 19). Compared with reported results for high temperature and high H_2 pressure conditions, this study obtained high hydrocarbon yields but under very low temperatures (<100 °C) and H_2 pressure (<1 atm) (shown in Fig. 2d and Supplementary Tables 4 and 5)[8,12,14,25–28].

The concentration of SiW_{12} ions is important for the HDO reaction under mild conditions. The results suggest that the hydrocarbon yield increased with SiW_{12} concentration and high yields of over 80% were achieved at a concentration of 25 mmol l^{-1} of SiW_{12} for phenol and guaiacol deoxygenation (Fig. 3a and Supplementary Fig. 20). These results show that a very low concentration of SiW_{12} can still improve the HDO. H_2 and N_2 gases mixed in different ratios were also used to further dilute the p_{H_2} in the reactor (Fig. 3b). The results indicate that an 85% hydrocarbon yield could still be obtained using the SiW_{12}–Pt/C catalyst system at 75 °C even at $p_{H_2} = 0.3$ atm (that is, a gas mixture of H_2:N_2 = 4:6), which suggests SiW_{12} can effectively transfer enough H_2 to the solution, even at a very low p_{H_2}. In other words, SiW_{12} can function as the H_2 buffer in the solution. The SiW_{12} and Pt/C catalyst system had a stable performance in the continuous experiments. As shown in Fig. 3c,d, for ten additions of phenol and five additions of guaiacol at ~30 and 40 minutes for each interval, no yield decrease was observed, which indicates a good performance of the SiW_{12} Pt/C catalyst over a long period.

Proposed mechanism of SiW_{12}-enhanced HDO

According to the literature, complete deoxygenation to form benzene in an aqueous solution is usually carried out under harsh conditions, such as near or above the water supercritical temperature[29,30]. This is because the aromatic C–O bond cleavage is much more difficult than deoxygenation of the hydrogen-saturated cyclohexanol[29,30]. The mechanism of benzene formation at a reaction temperature lower than 100 °C in this SiW_{12}–Pt/C catalytic system was studied by using density functional theory (DFT) calculations with the solvation model. Three different possible pathways of aromatic C–O bond cleavage were proposed and their reaction energy (ΔE_r) and activation energy (ΔE_a) were calculated (Fig. 4a and

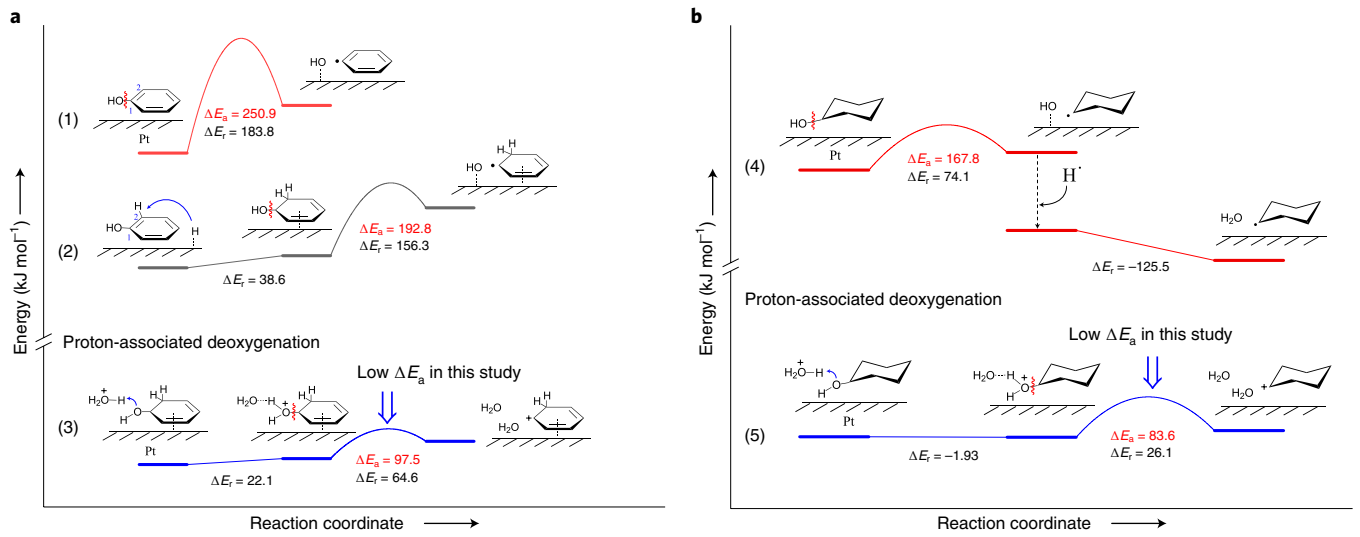

Fig. 4 | Proposed mechanism of SiW_{12}-induced HDO. a,**b**, Energy profiles of possible C–O bond-breaking pathways in phenol (**a**) and cyclohexanol (**b**) HDO on a Pt(111) surface. ΔE_r and ΔE_a were calculated by DFT with the solvation model.

Supplementary Fig. 21). A possible pathway is the traditional direct cleavage of the aromatic C–OH bond (dehydroxylation). The calculations show that the reaction is strongly endothermic ($\Delta E_r = 183.8$ kJ mol^{-1}) with a high activation energy of 250.9 kJ mol^{-1} (Fig. 4a, pathway (1)), which is similar to results reported in the literature[31–33]. The second pathway is deoxygenation after partial hydrogenation, which was also reported during HDO of phenol in the gas phase[32,33]. It was reported that the partial hydrogenation of the benzene ring starting from C_2 (the C atom next to the C–O bond) is the most favourable pathway due to the small activation energy[32]. With the hydrogenation of C_2, the delocalization of the C–O bond was reduced, which resulted in a decreased cleavage activation energy of 192.8 kJ mol^{-1} in this solvation model simulation, as shown in the pathway (2) in Fig. 4a. It can be seen that both pathways (1) and (2) are endothermic with a high activation energy.

Pathway (3) in Fig. 4a presents a proton-associated mechanism in the presence of SiW_{12}. It suggests that the SiW_{12}-associated proton plays a key role to greatly decrease the activation energy of C–O bond breaking in aqueous solution. It is well-known that polyoxometallates are superacids that have a much higher acidity than that of common organic and inorganic acids, such as H_2SO_4 or CF_3SO_3H. With the super acidic SiW_{12}, the partially hydrogenated phenol can be easily protonated to form an oxonium ion ($\Delta E_r = 22.1$ kJ mol^{-1} from our calculations) by combining with the hydronium ion H_3O^+ in water. Next, the dehydration of the protonated substrate occurs to yield a carbocation intermediate and water with a smaller activation energy of 97.5 kJ mol^{-1}. This proton-involved mechanism is obviously more energetically favourable compared with pathways (1) and 2). To verify the effect of acidity in the HDO, acids with different acidic strengths, which included CF_3SO_3H, HCl, H_2SO_4 and H_3PO_4, were selected to substitute SiW_{12} in this study. In a separate test, we also neutralized the SiW_{12} acid with NaOH to reduce the proton concentration and used this in the phenol HDO (Supplementary Fig. 22 and Supplementary Table 3). The experimental results show that the TOFs of hydrocarbon generation are strongly related to the acid strength: the stronger the acid strength of the reaction solution, the higher the reaction rate. Therefore, the high efficiency of phenol HDO in this study benefits not only from the hydrogen-buffer effect of SiW_{12}, which transfers hydrogen into the bulk solution, but also from the super acidity of SiW_{12}, which promotes the proton-associated dehydration for aromatic C–O bond breaking.

Phenol hydrogenation to give cyclohexanol also occurs simultaneously because the hydrogenation of the phenolic ring is favourable on Pt catalysts[32,33]. For the saturated hydrogenation product, cyclohexanol, C–O bond breaking is still the rate-limiting step that governs the formation of cyclohexane. With the SiW_{12}–Pt/C catalyst system, cyclohexanol can be deoxygenated to give cyclohexane through the preliminarily assumed dehydration of the protonated cyclohexyl oxonium ion. Although the actual deoxygenation mechanism is not fully confirmed and further research is necessary, our calculations suggest that the proposed pathway is energetically favourable, compared with a direct C–O bond cleavage of cyclohexanol, owing to the small activation energy (Fig. 4b and Supplementary Fig. 23). Note that in this SiW_{12}-induced HDO, H* was generated on the Pt catalyst surface due to electron transfer from the reduced $[SiW_{12}]^{5-}$ to a proton. The in situ generated hydrogen atom is active in the subsequent HDO, but it is supposed that SiW_{12} itself does not directly reduce the organic substance phenol. This is because it would be difficult for the neutral phenol molecule to directly receive an electron from the reduced SiW_{12} to form a phenol anion, which is a high-energy intermediate (97.45 kJ mol^{-1} higher than that of neutral phenol in the gas phase[34]).

Bio-oil compound upgrading under mild conditions

It has been known that lignin pyrolysis oil contains different aromatic derivatives of low molecular weight, which include 4-vinylguaiacol (3–7%), cresol (3–5%), syringol (3–5%), guaiacol (3–6%), isoeugenol (2–3%) and phenol (2–3%) and so on[35,36]. These major lignin bio-oil compounds with different –OH, –OCH_3, –CH_3, ethyl or propyl groups were used in this upgrading study under the mild hydrogenation conditions. The results of the hydrogenation of major lignin bio-oil compounds are shown in Fig. 5. The chemical properties of the substituted phenolic compounds can be affected by the combined effects of induced hyperconjugation and steric hindrance due to substituted groups on the benzene ring. However, the oxygen-containing groups can be efficiently removed to produce hydrocarbons with a yield of ~60–80%. The hydroxyphenyl (Ar–OH)- and catechyl (two *ortho*-OH)-structured derivatives have a high HDO rate under a low temperature of 75 °C. However, guaiacyl (one OH and one *ortho*-OCH_3) and trisubstituted syringyl (one OH and two *ortho*-OCH_3) units contained substrates that generally require longer reaction times (one hour) to reach a high hydrocar-

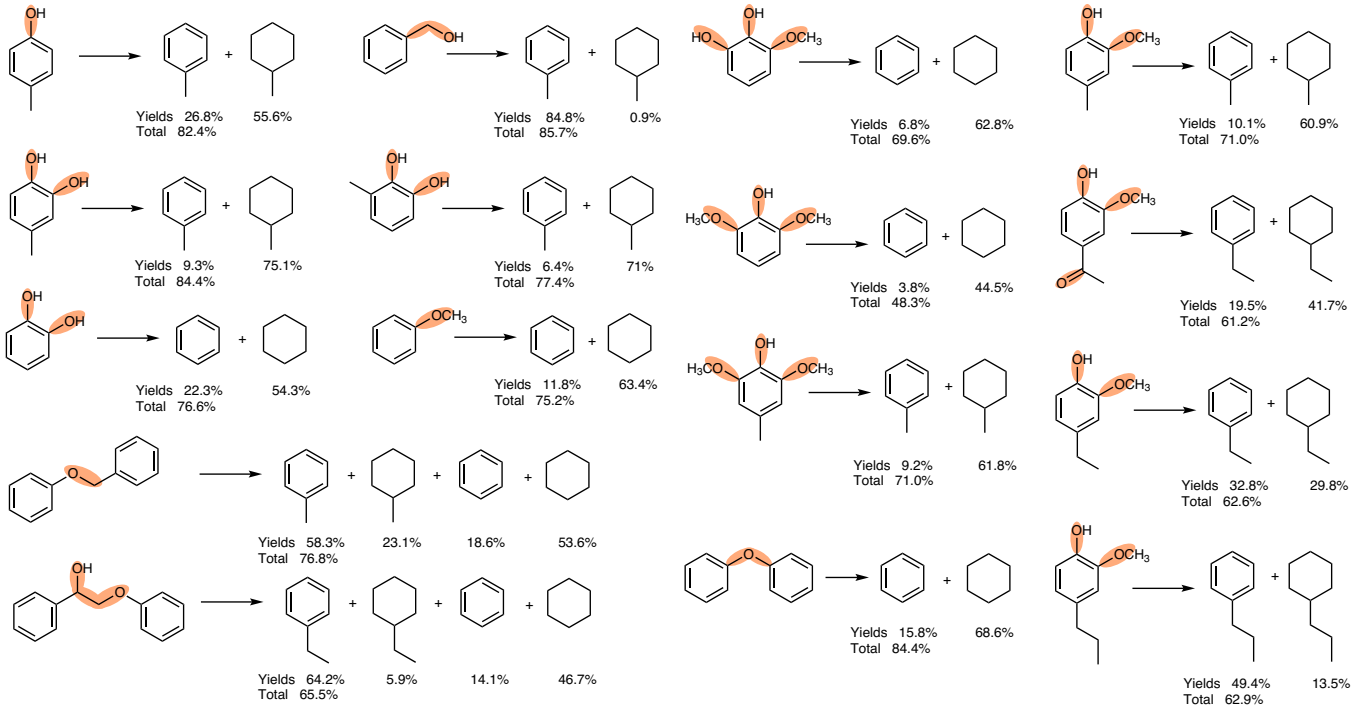

Fig. 5 | Upgrading of different functional-group-substituted compounds under mild conditions. The upgrading was carried out with a 0.05 mol l^{-1} SiW_{12} reaction solution and the Pt (5 wt%)/C catalyst ($p_{H_2} + p_{H_2O(g)} = 1$ atm at a temperature of 95 °C). The initial substrate concentration was 20 mmol l^{-1}, and the Pt-to-substrate ratio was fixed at 5% (mol:mol). The functional groups within the molecules that would be removed during the upgrading are shaded in orange. Gas chromatograms of the products and the required reaction times are shown in Supplementary Figs. 24–39. The yields were calculated using equation (2). It should be noted that for the compounds containing two benzene rings such as those shown in the bottom two rows, one mole substrate will yield two moles of hydrocarbons.

bon yield. In addition, the dimer model compounds that mimic the α-O-4, 4-O-5 and β-O-4 linkages in the lignin structure were also used under these mild conditions for HDO. The results show an efficient breakage of the aryl ether bond (Ar–O–Ar) and oxygen atom removal with this bifunctional catalyst system.

The methoxy functional group (–OCH_3) is abundant in lignin and lignin-derived oil. The cleavage of C–O–C_{methyl} bonds can proceed via three possible pathways (Fig. 6): (1) hydrolysis under acidic conditions to form a phenolic hydroxyl group and methanol, (2) hydrogenolysis of C–OCH_3, which results in the formation of a C–H bond and methanol, and (3) demethylation by hydrocracking of the CO–CH_3 bond to produce Ar–OH and methane. The acid-catalysed hydrolysis of the methoxy group has been reported[19,20]. In this study, however, the hydrolysis of the Ar–OCH_3 group was verified as negligible by heating anisole, as the model compound, with the SiW_{12} acid solution at 80 °C (without H_2), because no phenol product was observed. To investigate pathways (2) and (3), a HDO experiment in the SiW_{12}–Pt/C catalyst system using anisole was conducted, and the products methane, methanol and cyclohexanol detected (Supplementary Fig. 40). These results suggest that both pathways (2) and (3) are possible in HDO catalysed by SiW_{12}–Pt/C.

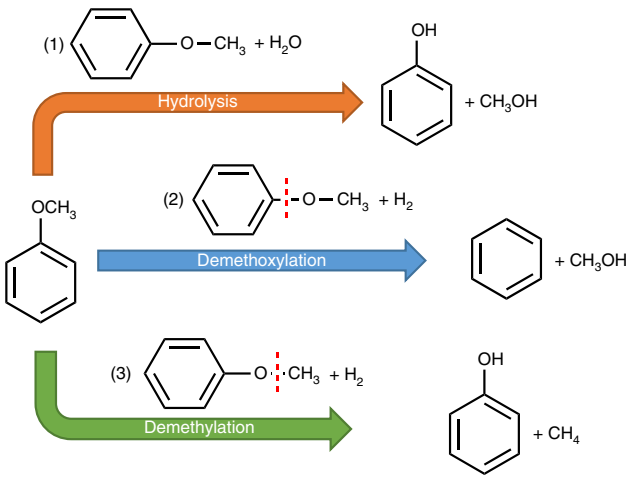

Fig. 6 | Three possible pathways for defunctionalization of the –OCH_3 group using anisole as a model compound. The red arrow represents the hydrolysis pathway of anisole with water, the blue arrow represents the demethoxylation pathway to produce methanol and benzene, and the green arrow represents the demethylation pathway to produce methane and phenol.

Conclusions

In conclusion, we have demonstrated a high-efficiency HDO of lignin-based bio-oil compounds catalysed by a triphase transfer catalytic system. In our experiments, high hydrocarbon yields of up to 90% were obtained from the upgrading of phenol and lignin bio-oil-based phenol derivatives under mild conditions of temperature lower than 100 °C simultaneously with hydrogen pressure lower than 1 atm. We used the low redox potential polyoxometalate acid, SiW_{12}, to enhance the H_2 transfer from the gas phase into the aqueous reaction solution under the very low hydrogen pressure. According to our calculations, as SiW_{12} is a superacid, the proton-associated deoxygenation mechanism through dehydration greatly decreases the reaction barrier for the splitting of C–O bonds, which realizes an efficient conversion of bio-derived phenolic oxygenates into hydrocarbons under mild conditions.

Methods

Materials. SiW_{12} was purchased from Alfa Aesar. The Pt/C catalyst was 5 wt% metal loaded on a matrix of activated carbon support, which was purchased from Sigma Aldrich. The organic substrates used in the electrolysis included phenol (Alfa Aesar, 99.5%), cyclohexanol (Alfa Aesar, >99%), benzyl alcohol (Sigma Aldrich, >99.8%), 4-methylcatechol (Alfa Aesar, 98%), guaiacol (Alfa Aesar, 98%), 3-methoxycatechol (Sigma Aldrich, >99%), *p*-cresol (Alfa Aesar, 98%), acetovanillone (Sigma Aldrich, >98%), diphenyl ether (Alfa Aesar, 99%), 2-methoxy-4-methylphenol (Alfa Aesar, 98%), catechol (Alfa Aesar, 98%), anisole (Sigma Aldrich, >99.7%), 2,6-dimethoxy-4-methylphenol (Sigma Aldrich, >97%), 4-(hydroxymethyl)-2,6-dimethoxyphenol (Alfa Aesar, 97%), 4-(3-hydroxypropyl)−2-methoxyphenol (TCI, 98%), 4-ethyl-2-methoxyphenol (Alfa Aesar, 98%), benzyl phenyl ether (Alfa Aesar, 97%), decane (Sigma Aldrich, >99%) and methanol (Sigma Aldrich, >99.9%). Dichloromethane (Sigma Aldrich, >99.8%) was used as the extraction solvent. High-purity water with a resistivity of 18.2 MΩ cm, obtained through a Milli-Q water purification system, was used for all the experimental procedures.

Electrochemical measurements. The reaction solution for the experiments was a 0.05 mol l^{-1} SiW_{12} (Alfa Aesar) solution with a suspension of 0.039 g of Pt/C catalyst (5 wt%, Alfa Aesar). The electrode potential changes during the H_2 reduction of SiW_{12} were measured in a closed beaker with a gas inlet and an outlet (Supplementary Fig. 1). A platinum black electrode was used as the working electrode and an Ag/AgCl electrode (BASi) was used as the reference electrode, which was connected to the reaction solution through a salt bridge. The potential difference between the working and reference electrodes was measured at room temperature by a Versa Stat 3 electrochemical working station (Princeton Applied Research). During the potential monitoring, N_2 or H_2 was flowed through the reaction solution with vigorous stirring.

The cyclic voltammetry measurements were taken on Versa Stat 3 electrochemical working station using a BASi Ag/AgCl reference electrode, a Pt wire working electrode and a Pt counter electrode. The cyclic voltammetry scanning was performed in a SiW_{12} solution (0.05 mol l^{-1}, without Pt/C), at room temperature with a scan rate of 100 mV s^{-1}. Electrode potentials were converted to the NHE scale using the equation $E_{NHE} = E_{Ag/AgCl} + 0.210$ V, where E_{NHE} is the potential versus the NHE and $E_{Ag/AgCl}$ is the measured potential versus the Ag/AgCl electrode.

Spectrophotometric measurement of $[SiW_{12}]^{5-}$. The concentration of $[SiW_{12}]^{5-}$ was determined by spectrophotometry. To obtain the calibration curve, 20 ml of SiW_{12} solution (0.1 M) without organics was reduced by electrochemical reduction treatment at 3 V for a charged time. A 1 m aliquot of the reduced SiW_{12} solution was taken out as a sample and then diluted to 10 mM for absorbance determination at 700 nm. Then, 15 m of the reduced SiW_{12} solution was taken out and titrated with potassium permanganate solution (first calibrated by a standard sodium oxalate solution). This process was repeated 3–4 times with different electrolytic reduction times. Thus, the standard curve of a 10 mmol l^{-1} SiW_{12} solution was obtained. To measure the concentration of $[SiW_{12}]^{5-}$ during H_2 reduction or electrolysis, 0.5 ml of the reaction solution was taken out at different time interval. The reduced SiW_{12} solution samples were diluted to 10 mmol l^{-1} and then were used for ultraviolet–visible spectroscopy measurement at 700 nm. Note that SiW_{12} can be re-oxidized by oxygen in air. Therefore, deoxygenated deionized water should be used and the entire test was done as quick as possible.

Measurement of hydrogen evolution from the $[SiW_{12}]^{5-}$ solution. $[SiW_{12}]^{4-}$ solution with a concentration of 0.05 mol l^{-1} (volume of 10 ml) was first reduced with the Pt/C catalyst in aqueous solution by H_2 at 20 °C. Then, the prereduced SiW_{12} solution was transferred by using a syringe into a sealed container, which had been purged by N_2 to replace the air before the solution transfer. The hydrogen evolution reaction occurred based on the electrolysis of SiW_{12} and the hydrogen evolution reaction, $[SiW_{12}]^{5-} + H^+ = [SiW_{12}]^{4-} + 1/2H_2\uparrow$. The hydrogen concentration inside the sealed container was measured by a Varian 490 micro-GC equipped with a Pora Plot U (10 m) column.

HDO of bioderived phenols. The phenol HDO was performed in a glass tube with magnetic stirring (Supplementary Fig. 6). Deionized water (9 ml), 0.72 g of SiW_{12} and 0.039 g of Pt/C (5 wt%) catalyst were added to form a suspended solution of the catalyst. The solution was heated to a particular temperature with stirring under a hydrogen atmosphere. After that, the SiW_{12} solution was reduced to reach equilibrium (about 10 min), 1 ml of phenol solution was added to the final concentrations of phenol (0.02 mol l^{-1}) and SiW_{12} (0.025 mol l^{-1}) with a Pt to phenol percentage of 5% (mol:mol). Hydrogen gas was flowed through the above the reaction solution with a flow rate of 6 ml min^{-1} and then passed through an ice-cold CH_2Cl_2 solution. The total pressure of the generated hydrogen and water vapour was maintained at 1 atm. For other HDO experiments with organic substrates, the added volume of the substrate solution varied but the total solution was 10 ml. The produced hydrocarbons were absorbed in the CH_2Cl_2 solution with a hydrogen flow. Other conditions, such as amount of SiW_{12}, temperature or H_2 flow rate were changed in different experiments. The continuous experiments were conducted by directly injecting the organic substrate (phenol and guaiacol) into the reaction system at 30 or 40 min intervals (the experimental set-up is shown in Supplementary Fig. 6). The produced hydrocarbons were continuously distilled out and collected for quantitative analysis. Our tests indicated that almost all (~85–90%) of the phenol or guaiacol can be converted into cyclohexane and benzene after 30 or 40 min. Therefore, our tests were actually done by injecting new organic substrate after the previous one was completely consumed.

The obtained hydrocarbon–CH_2Cl_2 solution (with the internal standard decane) was quantitatively analysed by gas chromatography (GC) (Agilent 7890) equipped with a VF-5ms (30 m × 0.25 mm × 0.25 μm) GC column and a flame ionization detector. The reacted aqueous solution was extracted by CH_2Cl_2 four times, and the obtained organic phase was dried by Na_2SO_4 and analysed by GC. The hydrocarbon yield was calculated by equation (2):

$$\text{Hydrocarbon yield} = \frac{\text{Total obtained moles of hydrocarbons}}{\text{Moles of reactant}} \times 100 \quad (2)$$

It should be noted that if the reactant contains two different benzene rings (such as benzyl phenyl ether and 2-phenoxy-1-phenylethanol), one reactant will produce two different hydrocarbon products. In such cases, equation (2) is still valid for calculating the individual product yield. However, for the total yield calculation, the denominator in equation (2) needs to be multiplied by two. On the other hand, if the reactant contains two of the same chemical rings (such as diphenyl ether), one mole of reactant can produce two moles of the same product. Therefore, the denominator in equation (2) would need to be multiplied by two not only for the total, but also for the individual product yield calculation. Methane is neglected because the yield measured was less than 1%.

Synthesis of 2-phenoxy-1-phenylethanol as a bio-oil model compound. Organic substrate 2-phenoxy-1-phenylethanol (β-O-4 linkage) was synthesized according to a reported method[38]. 2-Phenoxy-1-phenylethanone (TCI, 98%; 2.5 g, 11 mmol) was dissolved in methanol (100 ml) to form a solution. Sodium borohydride (Sigma Aldrich, 98%; 11 mmol) was added and stirred overnight at room temperature. After the reaction, a saturated solution of ammonium sulfate (200 ml) was added and then extracted by chloroform (200 ml). The organic layer was washed with water (100 ml twice) and then dried with anhydrate Na_2SO_4. The product was recrystallized from ethanol.

Catalyst characterization. The dispersion of the metal was investigated by transmission electron microscopy. Samples of the catalysts were ground and ultrasonically dispersed in ethanol. Drops of the suspensions were applied on a Cu–C grid and the measurements were carried out in a JEOL JEM-2011 electron microscope with an accelerating voltage of 120 keV. Statistical treatment of the metal particle size was done by counting at least 200 particles detected in several places on the grid. The morphology of the working electrode (activated carbon felt) before and after incorporating the catalyst was investigated by a scanning electron microscope (JSM-7500F from JEOL).

Calculations.

$$\text{Conversion} = \frac{\text{Moles of consumed substrate}}{\text{Initial moles of substrate}} \quad (3)$$

$$\text{Carbon balance} = \frac{\text{Moles of products detected by GC and unconsumed substrate}}{\text{Initial moles of substrate}} \quad (4)$$

(for phenol and guaiacol)

(The C_1 product (CH_4 and methanol) was not calculated in the carbon balance.)

The equations used for the TOF calculations of hydrocarbon production (TOF_{HC}) and substrate (phenol or guaiacol) consumption (TOF_{sub}) were:

$$TOF_{HC} = \frac{\text{Moles of produced hydrocarbons}}{\text{Time(h)} \times \text{dispersion of metal} \times \text{moles of active metal in the catalyst}} \quad (5)$$

$$TOF_{sub} = \frac{\text{Moles of consumed substrate (mmol)}}{\text{Time(h)} \times \text{Dispersion of metal} \times \text{Moles of active metal in the catalyst (mmol)}} \quad (6)$$

DFT computational methods. Periodic DFT calculations were carried out to explore possible reaction pathways by using the Vienna Ab Initio Simulation Package[39] along with a plane-wave basis set and projected-augmented wave pseudopotentials[40]. All the calculations used the Perdew–Burke–Ernzerhof[41] GGA XC functional. For the calculations, a four-layer Pt(111) slab was built with 4 × 4 atoms at each layer (the lattice constant of Pt slab was 3.967 Å). We used a 16 Å vacuum gap between the Pt layers to minimize the effects of interactions with atoms of the neighbouring layer. Geometries were relaxed until the force on each atom was smaller than 0.03 eV $Å^{-1}$ by using a quasi-Newton method. During the geometry relaxation of the Pt(111) slab, we simultaneously optimized both the cell

volume and ionic positions. After this initial geometry optimization, the cell shape and the volume were fixed in all subsequent calculations. The gamma-centred k-point meshes were 3×3×1, and the kinetic energy cutoff for the plane-wave basis set was set at 400 eV.

The adsorption energies of the adsorbed molecules were defined by:

$$-\Delta E = E_{\mathrm{ads+Pt(111)}} - E_{\mathrm{Pt(111)}} - E_{\mathrm{ads}} \quad (7)$$

where $E_{\mathrm{ads+Pt(111)}}$, $E_{\mathrm{Pt(111)}}$ and E_{ads} represent the energy of a Pt(111) slab with an adsorbed molecule, the energy of the empty Pt(111) slab and the energy of the adsorbate (guest molecule) in the gas phase, respectively. Zero-point energy and thermal contributions are neglected in this definition. With this convention, ΔE is positive when the adsorption is exothermic.

The reaction energies of hydrogenation and deoxygenation along the proposed reaction pathways were calculated as the energy difference between reaction products and reactants. The reaction energies (ΔE_r) and activation energy (ΔE_a) were defined by:

$$\Delta E_{\mathrm{r}} = E_{\mathrm{product}} - E_{\mathrm{reactant}} \quad (8)$$

$$\Delta E_{\mathrm{a}} = E_{\mathrm{transition}} - E_{\mathrm{reactant}} \quad (9)$$

where E_{product}, $E_{\mathrm{transition}}$ and E_{reactant} represent the total energies of the product, transition state and reactant either in a solvent or bound to the Pt slab. Positive and negative reaction-formation energies correspond to an energetically unfavourable process and an energetically favourable process, respectively.

Additionally, the parameter 'NELECT' was modified for charged-system modelling. To simulate the H_2O solvent environment, an implicit solvation model called VASPsol[42] was used to describe the effect of electrostatics, cavitation and dispersion on the interaction between a solute and solvent in all the calculations. The transition state between a reactant and product in an elementary step was determined by combination with the nudged elastic band method[43], which discretizes the reaction path into a series of structural images.

Data availability

The authors declare that the data supporting the findings of this study are available in the Article and Supplementary Information. Source data are provided with this paper.

Received: 18 February 2020; Accepted: 28 July 2020;
Published online: 7 September 2020

References

1. Armstrong, R. C. et al. The frontiers of energy. *Nat. Energy* **1**, 15020 (2016).
2. Liu, B. & Rajagopal, D. Life-cycle energy and climate benefits of energy recovery from wastes and biomass residues in the United States. *Nat. Energy* **4**, 700–708 (2019).
3. Savage, N. Fuel options: the ideal biofuel. *Nature* **474**, S9–S11 (2011).
4. Kunkes, E. L. et al. Catalytic conversion of biomass to monofunctional hydrocarbons and targeted liquid-fuel classes. *Science* **322**, 417–421 (2008).
5. Ragauskas, A. J. et al. Lignin valorization: improving lignin processing in the biorefinery. *Science* **344**, 1246843 (2014).
6. Duan, H. et al. Hydrodeoxygenation of water-insoluble bio-oil to alkanes using a highly dispersed Pd–Mo catalyst. *Nat. Commun.* **8**, 591 (2017).
7. Xia, Q. et al. Direct hydrodeoxygenation of raw woody biomass into liquid alkanes. *Nat. Commun.* **7**, 11162 (2016).
8. Saidi, M. et al. Upgrading of lignin-derived bio-oils by catalytic hydrodeoxygenation. *Energ. Environ. Sci.* **7**, 103–129 (2014).
9. Lin, Z., Chen, R., Qu, Z. & Chen, J. G. Hydrodeoxygenation of biomass-derived oxygenates over metal carbides: from model surfaces to powder catalysts. *Green Chem.* **20**, 2679–2696 (2018).
10. Mu, W., Ben, H., Ragauskas, A. & Deng, Y. Lignin pyrolysis components and upgrading—technology review. *BioEnergy Res.* **6**, 1183–1204 (2013).
11. Jing, Y., Dong, L., Guo, Y., Liu, X. & Wang, Y. Chemicals from lignin: a review of the catalytic conversion involving hydrogen. *ChemSusChem* **13**, 1–19 (2020).
12. Shafaghat, H., Rezaei, P. S. & Daud, W. M. A. W. Effective parameters on selective catalytic hydrodeoxygenation of phenolic compounds of pyrolysis bio-oil to high-value hydrocarbons. *RSC Adv.* **5**, 103999–104042 (2015).
13. Wang, H., Male, J. & Wang, Y. Recent advances in hydrotreating of pyrolysis bio-oil and its oxygen-containing model compounds. *ACS Catal.* **3**, 1047–1070 (2013).
14. Pritchard, J., Filonenko, G. A., van Putten, R., Hensen, E. J. M. & Pidko, E. A. Heterogeneous and homogeneous catalysis for the hydrogenation of carboxylic acid derivatives: history, advances and future directions. *Chem. Soc. Rev.* **44**, 3808–3833 (2015).
15. Kozhevnikov, I. V. Advances in catalysis by heteropolyacids. *Russian Chem. Rev.* **56**, 811–825 (1987).
16. Rausch, B., Symes, M. D., Chisholm, G. & Cronin, L. Decoupled catalytic hydrogen evolution from a molecular metal oxide redox mediator in water splitting. *Science* **345**, 1326–1330 (2014).
17. Yang, G. et al. The nature of hydrogen adsorption on platinum in the aqueous phase. *Angew. Chem. Int. Ed.* **58**, 3527–3532 (2019).
18. Singh, N. et al. Impact of pH on aqueous-phase phenol hydrogenation catalyzed by carbon-supported Pt and Rh. *ACS Catal.* **9**, 1120–1128 (2019).
19. Zhao, C., He, J., Lemonidou, A. A., Li, X. & Lercher, J. A. Aqueous-phase hydrodeoxygenation of bio-derived phenols to cycloalkanes. *J. Catal.* **280**, 8–16 (2011).
20. Güvenatam, B., Kurşun, O., Heeres, E. H. J., Pidko, E. A. & Hensen, E. J. M. Hydrodeoxygenation of mono- and dimeric lignin model compounds on noble metal catalysts. *Catal. Today* **233**, 83–91 (2014).
21. Ohta, H. et al. Low temperature hydrodeoxygenation of phenols under ambient hydrogen pressure to form cyclohexanes catalysed by Pt nanoparticles supported on H-ZSM-5. *Chem. Commun.* **51**, 17000–17003 (2015).
22. Alshehri, F., Feral, C., Kirkwood, K. & Jackson, S. D. Low temperature hydrogenation and hydrodeoxygenation of oxygen-substituted aromatics over Rh/silica: part 1: phenol, anisole and 4-methoxyphenol. *React. Kinet. Mech. Catal.* **128**, 23–40 (2019).
23. Chen, L., Fink, C., Fei, Z., Dyson, P. J. & Laurenczy, G. An efficient Pt nanoparticle–ionic liquid system for the hydrodeoxygenation of bio-derived phenols under mild conditions. *Green Chem.* **19**, 5435–5441 (2017).
24. Ohta, H. et al. Surface modification of a supported Pt catalyst using ionic liquids for selective hydrodeoxygenation of phenols into arenes under mild conditions. *Chem. Eur. J.* **25**, 14762–14766 (2019).
25. He, Z. & Wang, X. Hydrodeoxygenation of model compounds and catalytic systems for pyrolysis bio-oils upgrading. *Catal. Sustain. Energy* **1**, 28–52 (2012).
26. Long, W. et al. Different crystal form titania supported ruthenium nanoparticles for liquid phase hydrodeoxygenation of guaiacol. *J. Nanosci. Nanotechnol.* **18**, 8426–8436 (2018).
27. Si, Z., Zhang, X., Wang, C., Ma, L. & Dong, R. An overview on catalytic hydrodeoxygenation of pyrolysis oil and its model compounds. *Catalysts* **7**, 169 (2017).
28. Mäki-Arvela, P. & Murzin, Y. D. Hydrodeoxygenation of lignin-derived phenols: from fundamental studies towards industrial applications. *Catalysts* **7**, 265 (2017).
29. Garcia-Pintos, D., Voss, J., Jensen, A. D. & Studt, F. Hydrodeoxygenation of phenol to benzene and cyclohexane on Rh(111) and Rh(211) surfaces: insights from density functional theory. *J. Phys. Chem. C* **120**, 18529–18537 (2016).
30. Wang, M., Shi, H., Camaioni, D. M. & Lercher, J. A. Palladium-catalyzed hydrolytic cleavage of aromatic C–O bonds. *Angew. Chem. Int. Ed.* **56**, 2110–2114 (2017).
31. Yoon, Y., Rousseau, R., Weber, R. S., Mei, D. & Lercher, J. A. First-principles study of phenol hydrogenation on Pt and Ni catalysts in aqueous phase. *J. Am. Chem. Soc.* **136**, 10287–10298 (2014).
32. Liu, D. et al. Competition and cooperation of hydrogenation and deoxygenation reactions during hydrodeoxygenation of phenol on Pt(111). *J. Phys. Chem. C* **121**, 12249–12260 (2017).
33. Hensley, A. J. R., Wang, Y. & McEwen, J.-S. Phenol deoxygenation mechanisms on Fe(110) and Pd(111). *ACS Catal.* **5**, 523–536 (2015).
34. Jordan, K. D., Michejda, J. A. & Burrow, P. D. Electron transmission studies of the negative ion states of substituted benzenes in the gas phase. *J. Am. Chem. Soc.* **98**, 7189–7191 (1976).
35. Jiang, G., Nowakowski, D. J. & Bridgwater, A. V. Effect of the temperature on the composition of lignin pyrolysis products. *Energy Fuel.* **24**, 4470–4475 (2010).
36. Staš, M., Chudoba, J., Kubička, D., Blažek, J. & Pospíšil, M. Petroleomic characterization of pyrolysis bio-oils: a review. *Energy Fuel* **31**, 10283–10299 (2017).
37. Pourzolfaghar, H., Abnisa, F., Wan Daud, W. M. A. & Aroua, M. K. Atmospheric hydrodeoxygenation of bio-oil oxygenated model compounds: ae review. *J. Anal. Appl. Pyrol.* **133**, 117–127 (2018).
38. Zhang, C. et al. Promoting lignin depolymerization and restraining the condensation via an oxidation–hydrogenation strategy. *ACS Catal.* **7**, 3419–3429 (2017).
39. Kresse, G. & Furthmüller, J. Efficient iterative schemes for ab initio total-energy calculations using a plane-wave basis set. *Phys. Rev. B* **54**, 11169–11186 (1996).
40. Blöchl, P. E. Projector augmented-wave method. *Phys. Rev. B* **50**, 17953–17979 (1994).
41. Perdew, J. P., Burke, K. & Ernzerhof, M. Generalized gradient approximation made simple. *Phys. Rev. Lett.* **77**, 3865–3868 (1996).
42. Mathew, K., Sundararaman, R., Letchworth-Weaver, K., Arias, T. A. & Hennig, R. G. Implicit solvation model for density-functional study of nanocrystal surfaces and reaction pathways. *J. Chem. Phys.* **140**, 084106 (2014).
43. Henkelman, G., Uberuaga, B. P. & Jónsson, H. A climbing image nudged elastic band method for finding saddle points and minimum energy paths. *J. Chem. Phys.* **113**, 9901–9904 (2000).

Acknowledgements

W.L. thanks the RBI at Georgia Tech for scholarship support.

Author contributions

Y.D. and W.L. conceived the project and designed the experiments. W.L. performed the electrochemical measurement and HDO experiments. W.S. and W. Yang helped with the HDO experiments and product analysis by GC. W. You and W.L. conducted the DFT calculations of proton-induced mechanisms. A.K. performed GC–mass spectrometry analysis of the HDO products. Y.G. performed the catalyst characterizations.

Competing interests

The authors declare no competing interests.

Additional information

Supplementary information Supplementary information is available for this paper at https://doi.org/10.1038/s41560-020-00680-x.

Correspondence and requests for materials should be addressed to Y.D.

Reprints and permissions information is available at www.nature.com/reprints.

Publisher's note Springer Nature remains neutral with regard to jurisdictional claims in published maps and institutional affiliations.